PERGAMON

Journal of Structural Geology 24 (2002) 1777–1788

JOURNAL OF STRUCTURAL GEOLOGY

www.elsevier.com/locate/jstrugeo

Strain analysis from calcite e-twins in the Cameros basin, NW Iberian Chain, Spain

José M. González-Casado*, Carmen García-Cuevas

Departamento de Q.A. Geología y Geoquímica, Facultad de Ciencias, Universidad Autónoma de Madrid, 28049 Madrid, Spain

Received 28 February 2001; revised 2 August 2001; accepted 27 November 2001

Abstract

Calcite twins and *c*-axes from sparry grains that fill micro-veins were used to unravel the deformational history of the Cameros Massif, an inverted Mesozoic sedimentary basin located in the northwestern part of the Iberian Chain (Spain). Calcite *c*-axis and microvein orientations indicate the existence of two extension directions (NW–SE and NE–SW) during the basin formation probably related to the slip along two syn-sedimentary faults. Calcite e-twins were developed only in micro-veins from the frontal ramp area, i.e. in the northeast side of the basin, where the stresses were higher during the basin inversion. Twin analysis yields three different orientations (NW–SE, E–W and NE–SW) for the minimum horizontal extension direction (i.e. S_{hmax} under coaxial conditions), which suggests that the basin inversion was developed through several thrusting episodes, during which the frontal and lateral ramps of each one of these episodes are interchanged. Moreover, the perpendicularity between *c*-axes and the minimum extension directions suggests that the basin inversion was produced along the same faults that controlled the basin formation. The minimum extension directions deduced from e-twins are also consistent with the shortening directions established previously for the Tertiary evolution of the Iberian Chain, which suggest that the basin inversion involved several tectonic events during the Neogene. These results show the advantage of the combined *c*-axis and e-twins analysis to unravel deformational and kinematic histories.

Keywords: Calcite e-twins; Micro-veins; Cameros Massif; Iberian Chain; Strain analysis

1. Introduction

The mechanical twinning of calcite is one of the principal deformation mechanisms in coarse-grained limestones deformed at low-temperatures and pressures (Burkhard, 1993). In many cases, twinning strain is the only discernible deformation. The e-twin lamellae have been recognised as a deformational feature and crystallographic laws have been determined to use twinning strain in microstructural studies. All the analysis methods are based on the crystallographic twinning law, but only thin and straight twins (types I and II of Burkhard, 1993) are suitable for stress–strain analyses and their use is always limited to very small strains, which can be approximated by coaxial conditions. Strain measurements using e-twins are appropriate for rocks strained from 1 to <17%. Separation of several strain tensors from twin data sets has also been proved (e.g. Teufel, 1980; Ferrill 1991).

Turner (1953) and Weiss (1954) developed the first method for determining stress axis orientations from a population of e-lamellae in deformed calcareous rocks. Turner's method makes it possible to deduce geologically significant *T* (tension) and *C* (compression) directions from U-stage measurements of e-twin lamella and *c*-axis orientation. This method was modified and refined in order to establish the principal stress or strain directions and their magnitudes (e.g. Groshong, 1972; Spang, 1972; Laurent et al., 1981, 1990; Pfiffner and Burkhard, 1987; Nemcok et al., 1999). Groshong (Groshong, 1972, 1974; Groshong et al., 1984) developed the *calcite strain gauge technique*, a method that allows the determination of the complete strain tensor, which has been used by numerous authors to document strain due to intra-crystalline deformation by twinning in slightly to moderately deformed limestones (e.g. Wiltschko et al., 1985; Craddock and van der Pluijm, 1988; Kilsdonk and Wiltschko, 1988; Mosar, 1989; Evans and Dune, 1991; Ferrill, 1991; Ferrill and Groshong, 1993a,b; Hindle, 1997; Harris and van der Pluijm, 1998; González-Casado and García-Cuevas, 1999; García-Cuevas, 2000).

Consequently, e-twin determinations from calcite grains that fill micro-veins can be a useful tool for unravelling the

* Corresponding author. Tel.: +34-1-3973841; fax: +34-1-3974900.
E-mail address: g.casado@uam.es (J.M. González-Casado).

0191-8141/02/$ - see front matter
PII: S0191-8141(01)00166-3

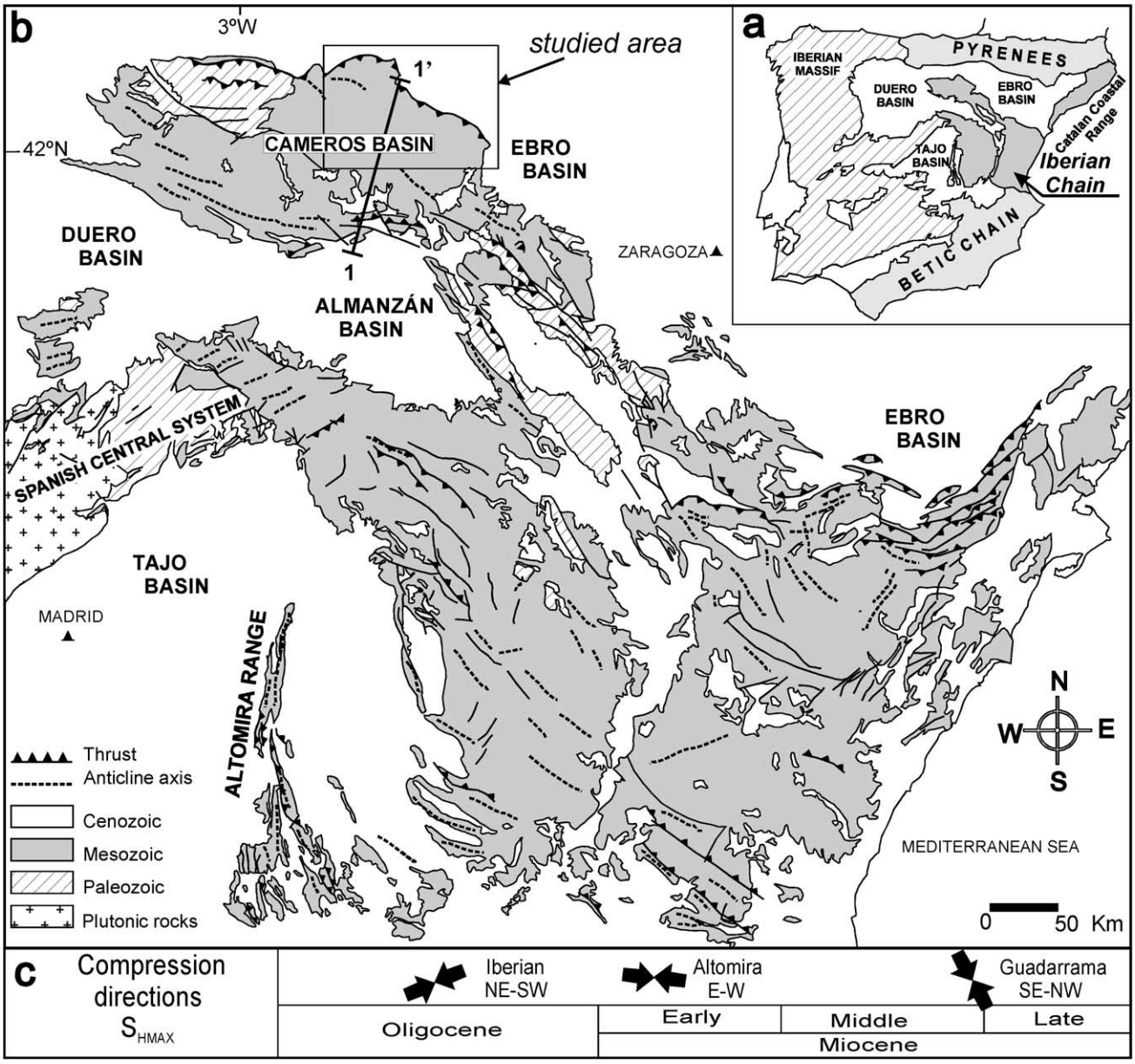

Fig. 1. (a) Tectonic map of Iberian Peninsula. (b) Simplified geological map of the Iberian Chain and location of the studied area. (c) Sketch of the gradual change in the compression direction in the Iberian Chain through the Tertiary.

deformational and kinematic history of a region (e.g. Spang and Groshong, 1981; Kilsdonk and Wiltschko, 1988; González-Casado and García-Cuevas, 1999; Craddock et al., 2000). A complete regional deformation history can be recorded in calcite micro-veins, which can be formed and strained during different regional tectonic events (e.g. González-Casado and García-Cuevas, 1999). The aim of this paper is to constrain the kinematic and deformational history of the Cameros basin, an inverted half-graben system, using data from calcite micro-veins (e-twin and *c*-axis). These data are also used to investigate the relationship between calcite twins and other tectonic structures (schistosity and folds) that are found inside this inverted basin.

2. Geological setting

The Cameros basin is located in the north-western sector of the Iberian Chain, an intraplate fold-and-thrust belt located in the eastern part of the Iberian Peninsula between the Pyrenees and the Betic Cordillera (Fig. 1a). The present mountain range was built up during the Alpine cycle and is mainly composed of a thick Mesozoic sedimentary cover, made of carbonate and siliciclastic marine and continental rocks, which lie unconformably on metamorphic Variscan basement.

The geological evolution of the Iberian Chain during the Mesozoic includes four extensional episodes: two main stages of rifting (Triassic and Late Jurassic–Early

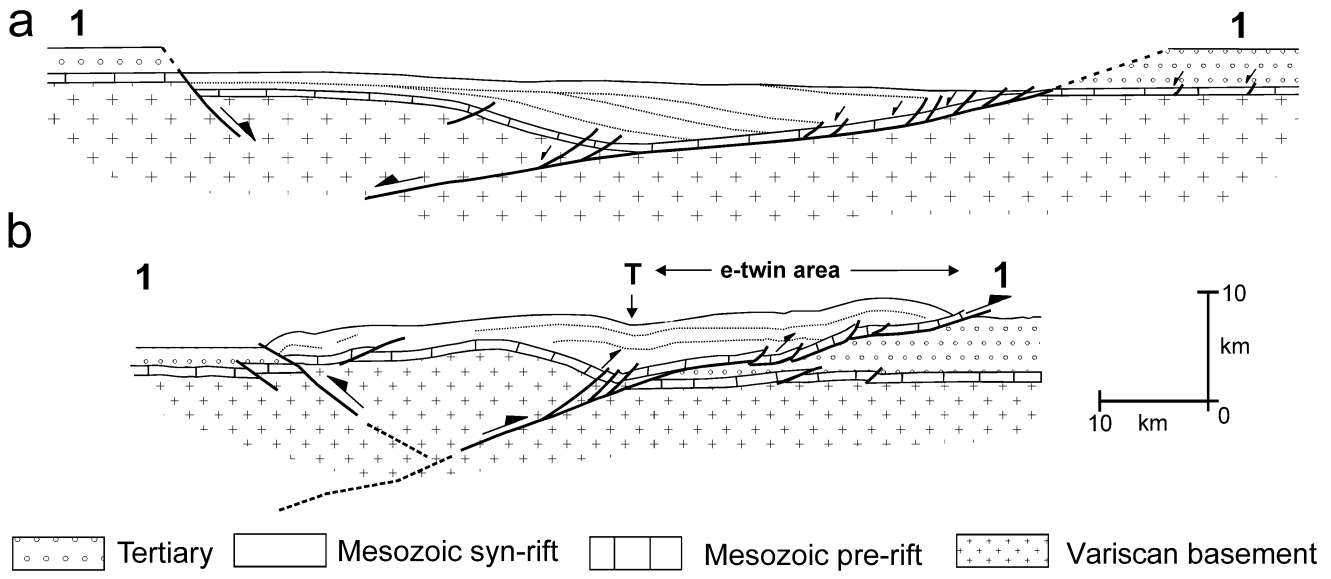

Fig. 2. Tectonic evolution of the Cameros basin. (a) Basin formation and distribution of the main sedimentary units. (b) Basin inversion (the figure is based in part on Guimerà et al. (1995) and Casas-Saínz and Simón-Gómez (1992)).

Cretaceous) followed by two episodes of thermal subsidence (Early–Middle Jurassic and Late Cretaceous) (e.g. Alvaro et al., 1979; Vilas et al., 1983; Salas and Casas, 1993). The Mesozoic cover thickness shows significant spatial variations inside this chain, defining several small basins. Many of the basins are related to dip-slip and wrench movement along old basement faults (post-Variscan) with NE–SW and NW–SE orientations, which were reactivated during the major rifting episodes (e.g. Alvaro et al., 1979; Arche and López-Gómez, 1996; González-Casado et al., 1996). Displacements along these faults gave rise to the development of the Cameros basin between the Late Jurassic and the Early Cretaceous.

The Iberian Chain was built-up during the Paleogene–Neogene interval in response to the compressional tectonics then occurring on the active margins of the Iberian Plate: the Pyrenees and the Betic Cordillera. Their structure is mainly characterised by folds and thrusts with two directions; the principal (NW–SE) is parallel to the longitudinal trend of the chain and the other is transverse (NE–SW) (Fig. 1b). These structures were formed during several tectonic episodes (Fig. 1c): the first (Paleogene, Iberian compression; Fig. 1c) was related to the tectonic activity on the north-eastern Iberian Plate margin (Pyrenees) and gave rise mainly to the NW–SE-trending structures (folds and large low-angle thrusts with SW and NE vergence; Fig 1b); the second (Neogene, Guadarrama compression; Fig. 1c) was associated with the activity on the south-eastern Iberian Plate margin (Betic Cordillera), which involved the development of NE–SW-trending folds and reverse faults, and it also produced strike-slip movements of the NW–SE faults. Generally, the NW–SE-trending low-angle thrusts within the Mesozoic cover have detachment levels located in Late Triassic beds (evaporites) and, in general, form the roof of a duplex thrust system in the basement (e.g. Capote, 1983; Viallard, 1983; Guimerà and Alvaro, 1990; Salas and Casas, 1993). Locally, a third N–S fold and thrust orientation is found in the Iberian Chain (e.g. Altomira Range; Fig. 1b). These structures have been related to an E–W compressive paleostress field (Capote, 1983; De Vicente 1988; De Vicente et al., 1996a) or with local stress field generated by the spatial and temporal superposition of major paleostress fields within the Pyrenees and Betics (Muñoz-Martín, 1997; Muñoz-Martín et al., 1998).

The Cenozoic sedimentary record (e.g. Calvo et al., 1993; De Vicente et al., 1996a) and the microstructural studies (e.g. Alvaro, 1975; Capote et al., 1982; Simón-Gómez, 1986; De Vicente, 1988; De Vicente et al., 1996b) also show that the evolution of the Iberian Chain has involved several deformation events, clearly separated in time (Fig. 1c): (a) NE–SW directed shortening during the Eocene (?) and Oligocene, probably in response to compression in the Pyrenean margin of the Iberian plate (Iberian compression). (b) A local episode of E–W shortening visible only in the Sierra de Altomira (Fig. 1b). (c) A NW–SE shortening episode (Guadarrama compression) that took place from the Middle to the Upper Miocene probably related to the continental deformation of the Betic Chain after the end of the Pyrenean activity. Thus, at least three compressive tectonic phases can be deduced in which the orientation of the horizontal maximum stress (S_{hmax}) changes from NE–SW, E–W to NW–SE during the Oligocene–Miocene interval (Fig. 1c).

2.1. The Cameros basin

The Mesozoic basin of Cameros (Fig. 1b) is an inverted

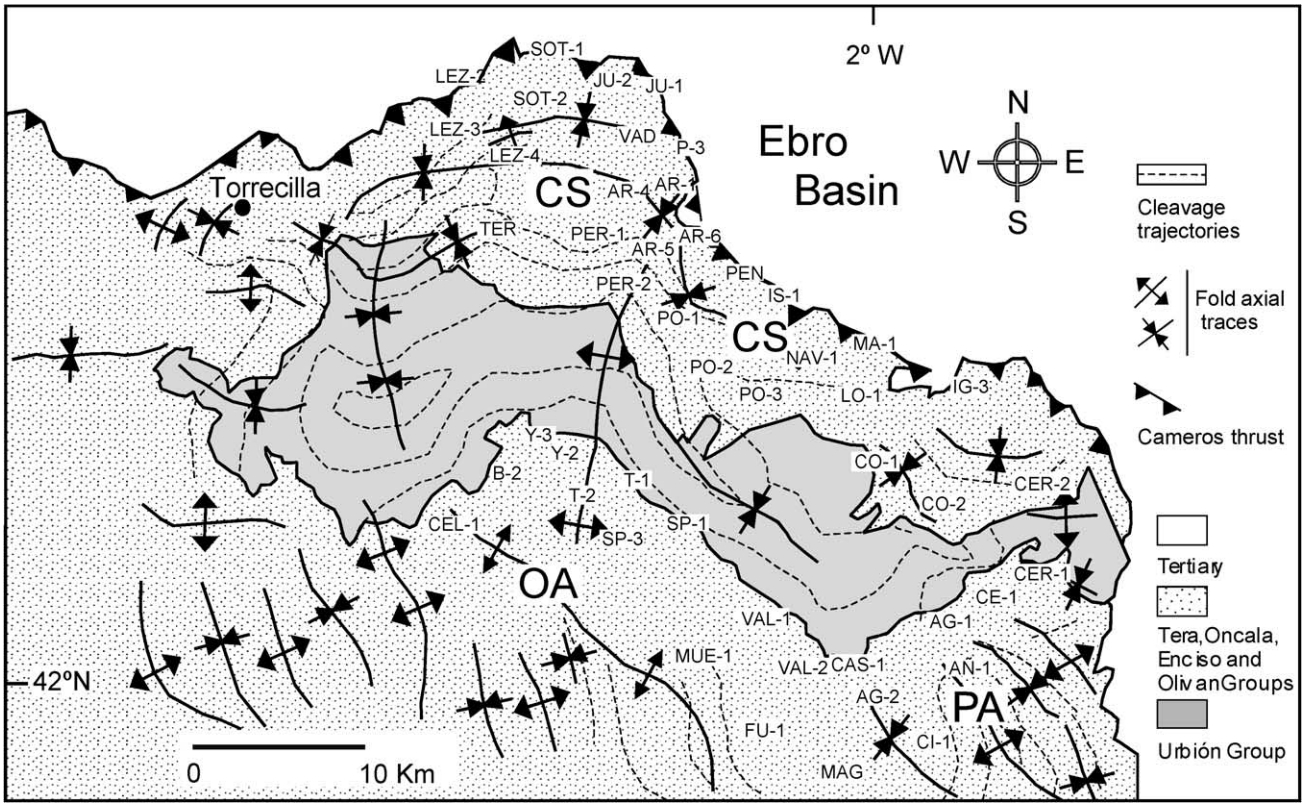

Fig. 3. Structural sketch of the northern part of Cameros. Map shows axial traces of folds; cleavage traces are based on Casas-Saínz and Gil-Imaz (1998) and sample points (Table 1). CS = Cameros synclinal. OA = Oncala anticlynal. PA = Pégado anticlynal.

basin originally developed during the Late Jurassic–Early Cretaceous continental rifting episode as an extensional–ramp basin. This basin was formed due to slip on a NW–SE-trending and S-dipping extensional fault buried several kilometres in the basement, although the depth of its sole is not well established (Fig. 2a). The displacement of the hanging wall to the south produced a synclinal basin over the ramp that progressively increased in size. The extension during the basin formation was >30 km (Guimerà et al., 1995). The basin was inverted during the Tertiary (Paleogene to Early–Middle Miocene) by means of a main northeast-directed thrust and a secondary south-dipping imbricate thrust system (Casas-Saínz, 1990; Casas-Saínz and Simón-Gómez, 1992; Guimerà et al., 1995) (Fig. 2b). The main thrust sheet includes the basin filling, its Mesozoic substratum and the Variscan basement (Casas-Saínz, 1990; Platt, 1990; Casas-Saínz and Simón-Gómez, 1992; Miegebielle et al., 1993; Guimerà et al., 1995). Both thrusts were probably active under a N–S compressional field that formed due to the convergence between the Spanish and the European plates (Casas-Saínz and Simón-Gómez, 1992). At present, the Cameros basin appears as a pop-up structure where the Mesozoic rocks are thrust more than 30 km over the Tertiary sediments of the Ebro basin (Casas-Saínz, 1990; Guimerà et al., 1995) (Fig. 2b).

Inside this basin three different tectono–stratigraphic units can be identified:

1. The Mesozoic *pre-rift* units, which correspond to Triassic rocks of Germanic facies and marine Jurassic sediments (Hettangian–Kimmeridgian). The Triassic lies unconformably over the Variscan basement, which is made up of low-grade metamorphic rocks of Precambrian to Ordovician age. The Triassic lutite and gypsum beds are the regional detachment level of the Mesozoic sedimentary cover (Guiraud and Séguret, 1985; Casas-Saínz, 1990; Casas-Saínz and Simón-Gómez, 1992; Guimerà et al., 1995).
2. The Mesozoic *syn-rift* infill. The basin record (Fig. 2a) consists of more than 5000 m of siliciclastic and carbonate sediments (Tithonian–Early Albian megacycle) bounded by two unconformities (Mas et al., 1993). These sediments show predominantly continental origin (alluvial and lacustrine systems) with only minor marine intercalations. The Cameros basin is characterised by very high subsidence and sedimentation rates during the rifting. Five lithostratigraphic groups (Tera, Oncala, Urbion, Enciso and Olivan Groups; Tischer, 1966) collectively termed ‘Wealdian’, comprising six depositional sequences, each bounded by unconformities (Mas et al., 1993), are recognised.
3. The Mesozoic *post-rift* units. This Late Albian–Maastrichtian sequence is more than 1000 m thick and

Table 1
Results of calcite e-twin analysis (*Groshong's Strain Gauge Technique*): (a) for 33 samples of syn-rift limestones and (b) for four samples of the pre-rift limestones. e_1, e_2, and e_3 refer to percent elongation (negative values indicate shortening) and orientation (plunge and plunge azimuth) of maximum (e_1), intermediate (e_2) and minimum (e_3) elongation direction. $\sqrt{(J2)}$ is the square root of the second invariant of the strain tensor (percent strain). *M* is the number of twins analysed and *n* is the number of twins used to establish the strain tensor

Sample	Principal strains (percent elongation)			$\sqrt{(J2)}$	Standard 'error'	*M*/*n*
	e_1	e_2	e_3			
(a)						
AG 2	20/178 (2.721)	69/351 (0.682)	02/087 (−3.403)	3.119	0.526	51/41
AR 1	12/165 (1.248)	76/008 (−0.250)	05/256 (−0.999)	1.144	0.826	33/27
AR 4	40/131 (1.567)	39/263 (0.280)	26/016 (−1.847)	1.724	0.615	52/42
AR 5	39/219 (0.974)	50/053 (−0.175)	07/315 (−0.799)	0.899	0.196	53/43
AR 6	44/203 (1.304)	33/075 (−0.129)	29/325 (−1.175)	1.244	1.122	25/20
CE 1	77/077 (1.951)	13/274 (0.633)	04/184 (−2.584)	2.332	2.086	12/10
CEL 1	11/020 (0.245)	13/113 (−0.005)	73/253 (−0.240)	0.242	0.026	54/44
CER 2	67/304 (0.274)	22/116 (−0.031)	03/207 (−0.244)	0.793	0.369	53/43
CI 1	79/340 (0.228)	10/174 (0.004)	02/083 (−0.232)	0.230	0.021	42/34
CO 2	18/151 (0.234)	41/044 (0.132)	43/258 (−0.366)	0.321	0.065	32/26
FU 1	76/065 (1.361)	06/179 (−0.367)	13/271 (−0.999)	1.220	0.407	43/35
IG 3	68/086 (0.256)	21/251 (−0.063)	05/343 (−0.193)	0.231	0.031	15/12
JU 2	84/086 (1.436)	06/253 (−0.599)	01/343 (−0.838)	1.250	0.415	27/22
LEZ 2	43/102 (1.782)	47/281 (−0.603)	01/012 (−1.179)	1.570	0.475	50/40
LEZ 3	25/073 (0.734)	64/271 (−0.100)	07/166 (−0.634)	0.689	0.144	25/20
LEZ 4	36/225 (1.409)	53/032 (0.241)	06/130 (−1.651)	1.544	0.348	55/44
LO 1	14/267 (0.314)	52/158 (−0.046)	34/007 (−0.268)	0.294	0.102	22/18
MAG	09/102 (0.441)	24/008 (0.116)	64/210 (−0.557)	0.509	0.106	47/38
MUE 1	46/347 (0.216)	44/162 (0.060)	03/255 (−0.276)	0.252	0.051	35/28
NAV 1	33/325 (0.747)	05/232 (−0.259)	56/135 (−0.489)	0.657	0.119	48/39
PER 1	77/105 (5.763)	13/297 (−2.398)	03/206 (−3.366)	5.014	0.956	16/13
PER 2	38/200 (3.528)	43/063 (−0.725)	23/309 (−2.803)	3.227	3.672	25/20
PO 1	83/014 (0.649)	03/260 (−0.208)	06/170 (−0.441)	0.574	0.173	19/16
PO 3	08/094 (4.413)	80/236 (−1.601)	06/003 (−2.812)	3.869	1.116	51/42
SOT 1	67/038 (0.839)	15/166 (−0.116)	17/261 (−0.722)	0.787	0.143	35/28
SOT 2	52/005 (0.641)	06/103 (−0.126)	38/197 (−0.516)	0.589	0.240	13/11
SP 1	38/155 (1.891)	32/035 (0.599)	35/278 (−2.491)	2.252	0.427	50/40
SP 3	60/203 (2.606)	19/330 (−0.096)	22/068(−2.509)	2.559	0.352	43/43
T 1	04/143 (0.422)	79/256 (0.008)	10/052 (−0.429)	0.426	0.084	45/36
TER	51/117 (1.847)	38/308 (0.480)	05/214 (−2.327)	2.128	0.970	27/22
VAL 1	40/001 (0.246)	43/218 (−0.072)	20/108 (−0.173)	0.219	0.111	18/15
VAL 2	40/183 (0.112)	46/030 (−0.008)	14/285 (−0.104)	0.108	0.029	36/29
Y 2	08/261 (1.273)	69/009 (−0.337)	20/168(−0.895)	1.132	0.713	23/19
(b)						
IS 1	26/272 (0.296)	64/099 (0.008)	03/003 (−0.305)	0.300	0.171	36/29
JU 1	28/009 (0.556)	19/269 (0.021)	56/149 (−0.577)	0.567	0.153	49/40
MA 1	84/195 (3.762)	02/083 (−1.443)	06/353 (−2.319)	3.287	0.943	27/22
P 3	08/081 (0.052)	78/214 (0.009)	08/350 (−0.062)	0.058	0.019	28/23

is mainly represented by siliciclastic continental deposits (Utrillas Sands Formation).

During the basin inversion, the Cameros basin moved like a solid block (Casas-Saínz and Simón-Gómez, 1992) because of the presence of a detachment level on the Late Triassic evaporite beds (Keuper) and by the rigid behaviour of the basin sedimentary pile. This behaviour was in part due to the hardening caused by the low-grade metamorphism that took place here during the Early Cretaceous (Golberg et al. 1988; Casquet et al., 1992; Mantilla-Figueroa, 1999). In detail, gentle kilometric-scale folds (e.g. the northern Cameros Synclinal, the Oncala Anticlynal or the Pégado Anticlynal; Fig. 3) and several minor fold swarms suggest that the entire basin pile experienced modest internal deformation.

A penetrative cleavage is also observed locally within the basin (Tischer, 1966; Guiraud and Séguret, 1985), the origin and characteristics of which are under debate (e.g. Casas-Saínz and Gil-Imaz, 1998; Gil-Imaz, 1999; Mantilla-Figueroa, 1999). The cleavage distribution is apparently controlled by lithology, because it is present in *pre-* and *syn-rift* materials, except for the Early Jurassic massive limestones. This microstructure is more pervasive in the central part of the basin, on a 5–6-km-wide zone between the lower limit of the Urbion Group and the upper limit of

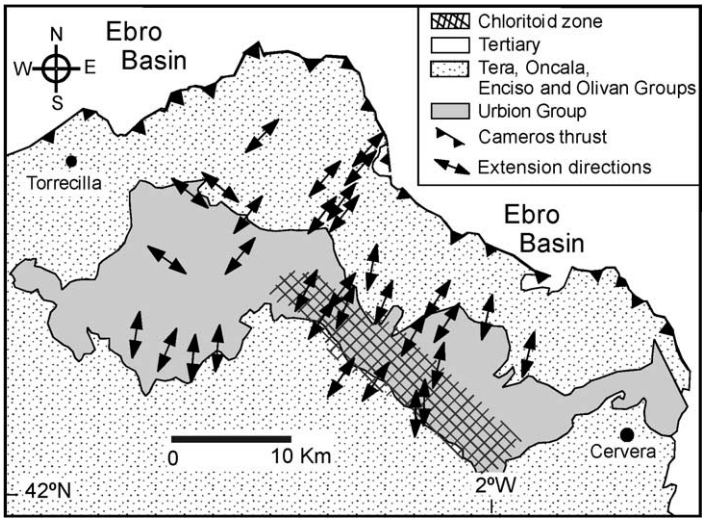

Fig. 4. Extension directions deduced from tension gashes filled with quartz by Guiraud and Séguret (1985). The chloritoid zone is also represented (from Mantilla-Figueroa (1999) and Mata (1997)).

the Oncala Group, where the rocks also exhibit a higher metamorphic grade (chloritoid zone; Guiraud and Séguret, 1985; Mata, 1997; Mantilla-Figueroa, 1999; Fig. 4). Cleavage is less pervasive in the north and tends to disappear toward the south.

Despite the shortening that took place during the basin tectonic inversion, syn-rift sediments preserve some extensional structures, mainly tension gashes and micro-veins, which have been traditionally used to establish the extension direction during the basin formation (e.g. Guiraud and Séguret, 1985; Fig. 4).

3. Method

In this work we analyse the rock deformation history using calcite twins from sparry grains that fill micro-veins (see Burkhard (1993) for a detailed review of methodology). More than 60 oriented samples were collected from the pre- and syn-rift Mesozoic rocks that host calcite veins inside this basin. We determined for each grain: e-twin orientations, *c*-axis orientation, number of twins, average thickness of twins and grain width using a petrographic microscope with a U-stage. Measurements were made on two orthogonal thin sections in order to avoid the U-stage 'blind spot'. Data from the two sections of the same sample were rotated into a common reference frame and combined before calculating the final result.

Strain ellipsoid principal axis orientations were calculated using the *strain gauge technique* developed by Groshong (see Groshong (1972, 1974) for a detailed description of this analysis method), which yields good estimates in slightly to moderated deformed limestones (Burkhard, 1993), through the computer program developed by Evans and Groshong (1994). This method establishes a strain tensor (principal strain axis orientation and relative magnitudes) for each sampling point that statistically best matches the observed e-twin population. The strain tensor is calculated by means of a least-square technique, which accounts for a maximum number of twins. In a second stage, grains that are not properly oriented for twinning with respect to this tensor are identified by calculating the value of the strain in each twin set and the deviation of this strain from the complete strain tensor (negative expected values, NEV). The percentage of NEV is a direct measure of the homogeneity of the twin data set. For instance, a high percentage of NEV ($>40\%$) could indicate in sedimentary rocks non-coaxial deformation or superimposed deformations. In this work after removal from the data set of those grains that show the largest deviations from the calculated expected values, a second (final) strain tensor was calculated.

4. Results and discussion

In the Cameros basin region, macroscopic dilation veins (extension, or mode I, fractures) are abundant and are filled with quartz or calcite depending on whether they are hosted in lutite or in carbonate levels (e.g. Marqués et al., 1996). Mantilla-Figueroa (1999) established the hydrothermal origin of these structures and García-Cuevas (2000), through cathodoluminiscence analyses, concluded that the filling took place during a single and short-lived episode. The calcite micro-veins studied here show variable widths that range between 0.05 mm and 2 cm. The individual sparry grains have sizes varying between 50 and 3000 μm. The shape of calcite crystals are moderately elongate (length/width ratio of grains <10). The existence of medial sutures suggests syntaxial crystal growth. Generally, the calcite *c*-axes are oriented normal to the vein borders and the opening trajectories deduced from

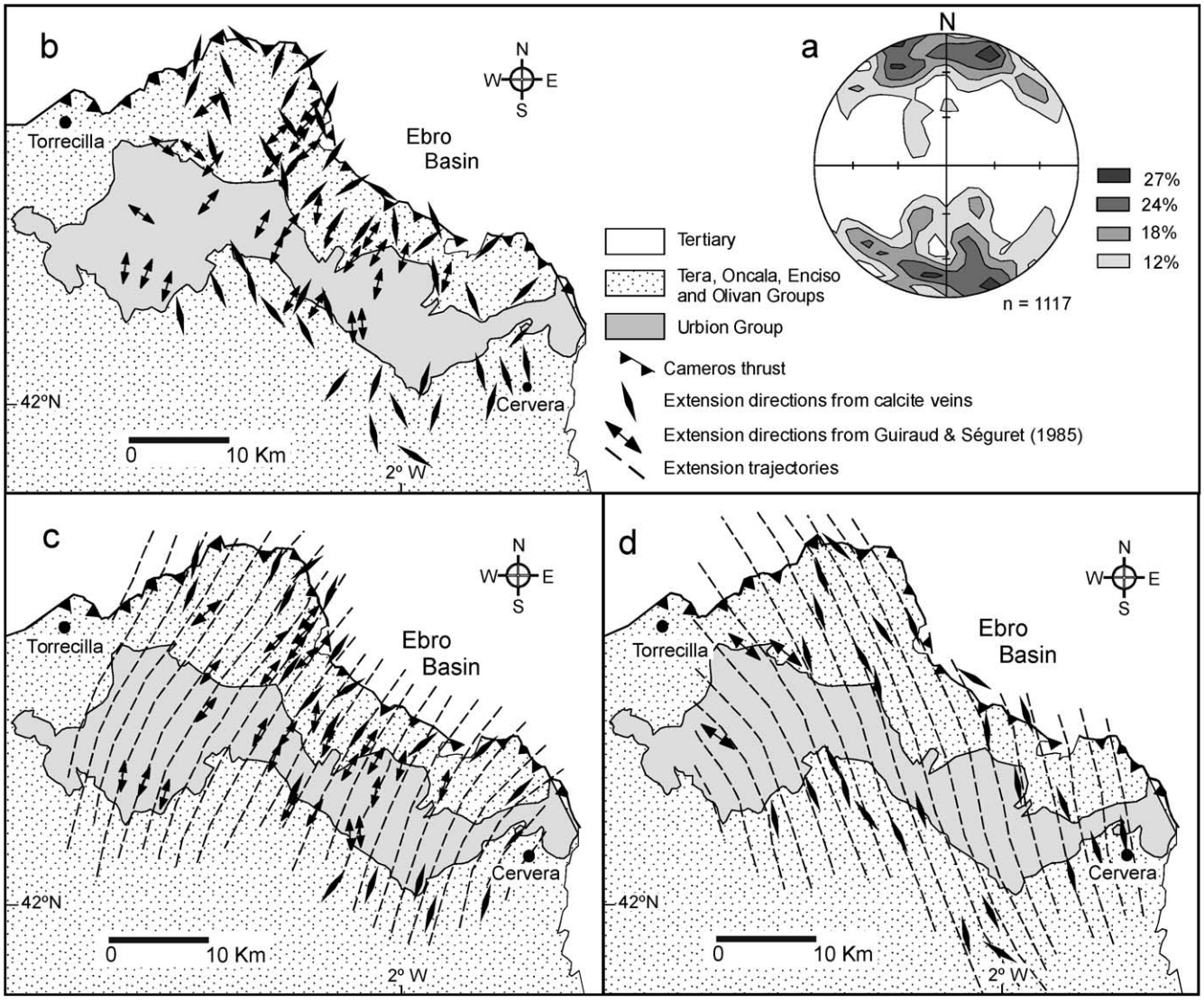

Fig. 5. Extension directions deduced from calcite veins. (a) Stereonet (Schmidt projection, lower hemisphere) showing calcite *c*-axis distribution. (b) Extension directions during vein opening deduced from calcite *c*-axes (this work) and tension gashes filled with quartz (Guiraud and Séguret, 1985). Vein opening trajectories are obtained by applying the interpolation method of Lee and Angelier (1994) for the NE–SW (c) and NW–SE (d) episodes. The spatial distribution shows the regional character of both events.

originally adjacent points on the opposite vein walls are perpendicular to the vein walls. Thus, the precipitation of calcite within mode I fractures is corroborated by the geometrical (orthogonal) relationship between calcite *c*-axes and fracture walls. Then the vein and the *c*-axis orientations were used here to establish the vein opening direction. Nevertheless, in some minor cases, calcite *c*-axes are oriented slightly oblique to the vein borders.

4.1. Extension direction during micro-vein formation

Guiraud and Séguret (1985) attributed the vein opening process to the tectonic extensional event associated with basin development during the Mesozoic (i.e. the syn-rift episode) and inferred two extension directions from vein wall orientations. They established a primary NE–SW extension direction and a secondary NW–SE direction (Fig. 4). Guimerà et al. (1995), in contrast, suggested that the orientation of the basin boundaries influences the extension direction locally, and proposed that towards the basin centre the extension direction tends to be oriented NNE–SSW to N–S when based on measurements away from basin-bounding faults.

We use the orientation of calcite *c*-axes to establish the extension direction during the micro-vein opening, and the orientation of more than 1000 *c*-axes from micro-veins hosted by syn- and pre-rift limestones were considered (Fig. 5a). The results yield two main subhorizontal maxima defining NNW–SSE and NNE–SSW extension directions (Fig. 5a). These extension directions show an homogeneous

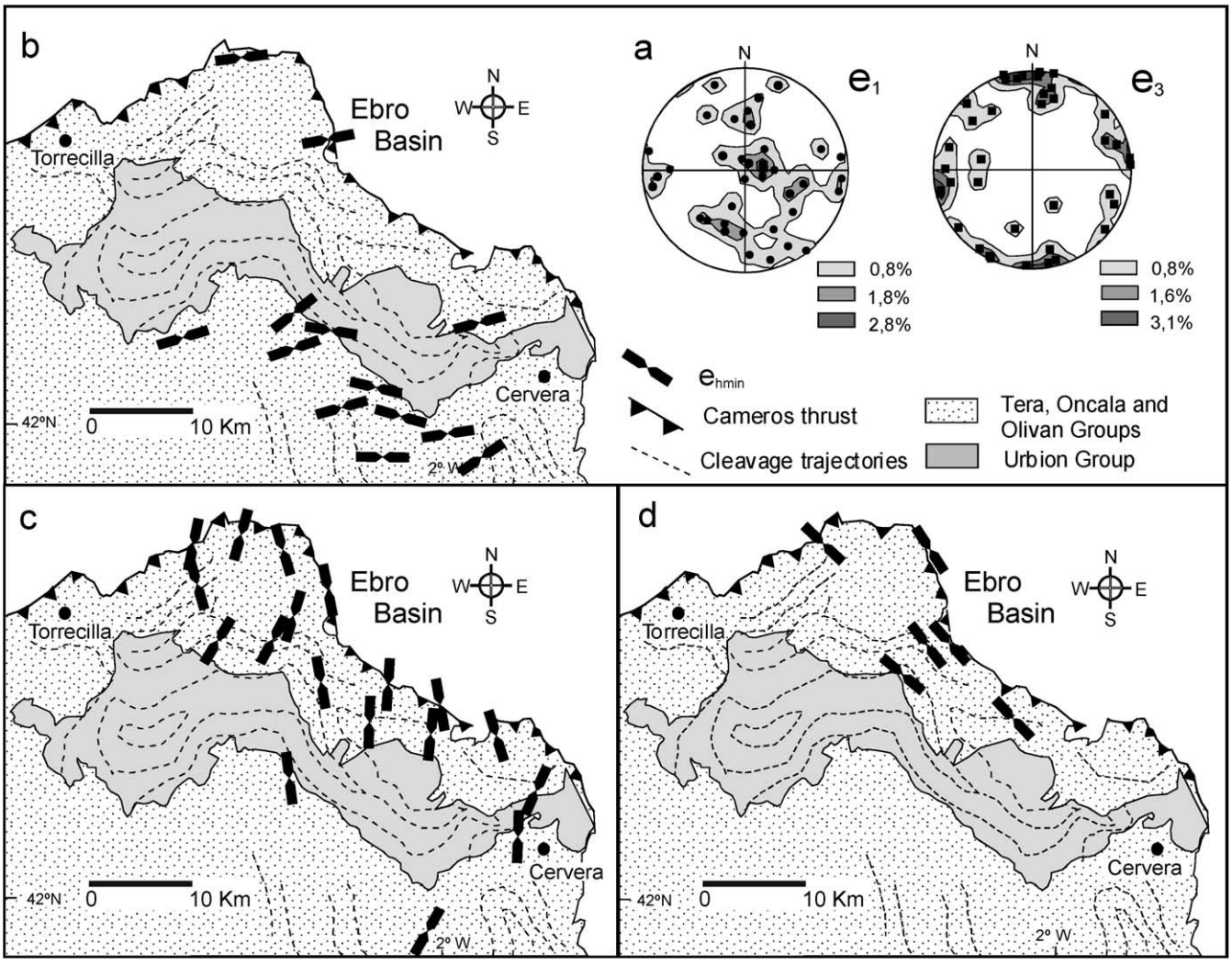

Fig. 6. Maximun shortening directions deduced from calcite twins. (a) Stereonets (Schmidt projection, lower hemisphere) showing strain e_1 and e_3 axes distribution for all the sites (for location see Fig. 3). (b), (c) and (d) show the E–W, N–S and NW–SE directions of maximum horizontal shortening, respectively.

distribution in the studied region (Fig. 5c and d), which suggests the existence of two different regional vein opening episodes.

These extension directions show an inverse order from those defined by Guiraud and Séguret (1985), who considered the NE–SW direction to be the principal extension and attributed the other directions to local heterogeneity. However, the detailed analysis of *c*-axis maxima in each site (Fig. 5c and d) suggests two superimposed extension directions.

The *c*-axis orientation in each site yields the maximum horizontal extension direction (e_{hmax}, i.e. the minimum horizontal stress, S_{hmin}, under coaxial deformation). The transformation of local scattered directional data into a map of e_{hmax} trends was carried out, applying the distance weighting method of Lee and Angelier (1994), which is based on an inverse distance weighting function, the degree of smoothness of trajectories being controlled by the power value and threshold distance. The interpolation includes those data of Guiraud and Séguret (1985). The homogeneous distribution of both opening directions (Fig. 5c and d) suggests that, after or during the last episodes of the basin formation, two regional extensional episodes took place. The cross-cutting relationship of the veins and the abundance of NE–SW *c*-axis maxima in veins hosted on the Mesozoic pre-rift rocks (i.e. in the marine Jurassic limestones) suggest that probably this extension occurred prior to the NW–SE extension. Taking into account that the geometry of the Cameros basin at depth consists of basement faults with NW–SE and NE–SW trends (e.g. Casas-Saínz, 1990; Casas-Saínz and Simón-Gómez, 1992), it is possible to infer that vein opening could be related to the movement on these faults.

4.2. Micro-vein deformation

Calcite twinned grains were abundant only at 37 sites from among the 94 sites studied (García-Cuevas, 2000),

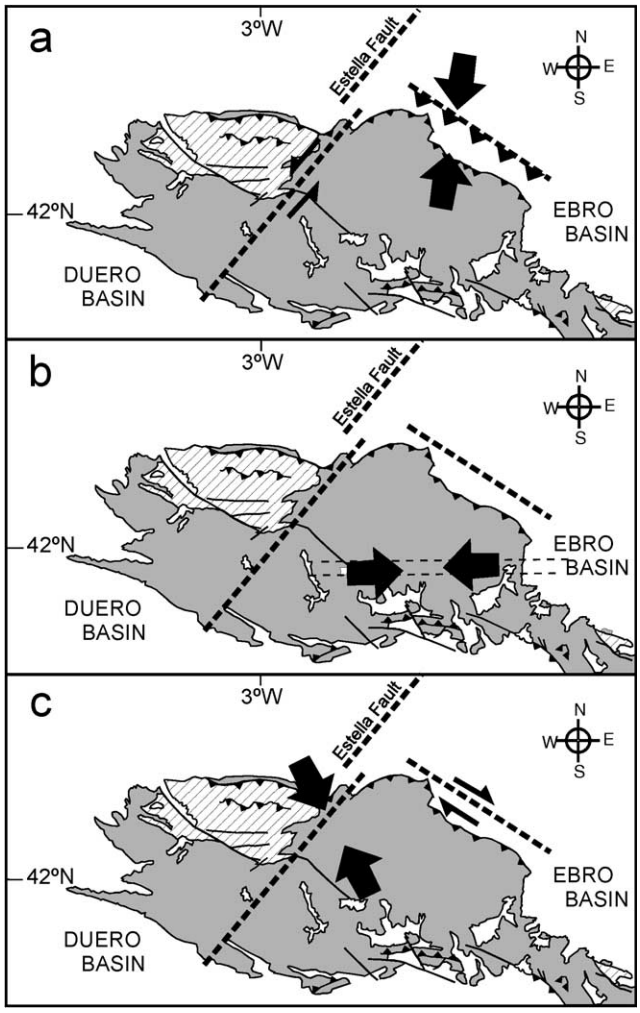

Fig. 7. Geological sketch of the Cameros basin during the tectonic episodes leading to the e-twin formation. (a) Iberian, (b) Altomira and (c) Guadarrama tectonic episodes. Arrows represent the main compression directions; also represented are the inferred slip motion of these faults that controlled the inversion of this basin.

which span the zone between the northern and southern borders of the Cameros Massif (Fig. 3). Thirty-three sites are from the syn-rift beds and four sites from pre-rift limestones. Sites with abundant twinned grains are located only in the northwestern side of the basin, i.e. next to the basin leading edge. Thus, twinning is only abundant in the thrusting wedge (Fig. 2b). Thin (<1 μm) and type I (thin and straight) twins are dominant and are characteristic of calcite deformed below 200 °C (Ferrill, 1991, 1998; Burkhard, 1993).

Twinning strain was calculated using the *strain gauge technique* (Groshong, 1972, 1974; Groshong et al., 1984). Results of the calcite e-twin analysis for each of the 39 samples are shown in Table 1. Normally, the percentage of NEV are $<40\%$, which indicates that the strain by twinning took place in a single event. Only in two samples, NEV are $>40\%$ (samples LEZ-2 and Y-2). The maximum shortening values (percent elongation of e_3 axis) is small (average -1.13%), with maximum and minimum values of -3.40% and -0.06%. According to the square root of the second invariant of the strain tensor ($\sqrt{J2}$) the average of elongation by twinning is 1.28% with maximum and minimum values of 5.01 and 0.05.

The orientation of the principal strain axes e_1 (maximum elongation) and e_3 (minimum elongation) show two relationships: frequently e_3 and e_1 exhibit low plunges, so the twinning appears to be associated with a regional tectonics of transcurrent character, and only in some cases e_3 axes are subhorizontal and e_1 axes are oriented subvertical (Fig. 6a). These orientations suggest that twinning does not reflect the extensional episodes related to the basin formation, but rather reflects the compressional events related to the basin inversion. The location of the twins only in the thrusting wedge (Fig. 2b) and the calculated values of shortening by twinning, similar to those seen in previous studies from thin-skinned thrust belts (e.g. Groshong, 1975; Spang and Groshong, 1981; Groshong et al., 1984; Ferrill, 1991; Craddock et al., 2000) also suggest this interpretation.

In order to show the relationship between the calcite twin strain results and the tectonic structures of this region, we have calculated the minimum horizontal extension direction for each site (e_{hmin}). Results yield three subhorizontal maxima oriented E–W, N–S and NW–SE (Fig. 6b–d). NW–SE and E–W e_{hmin} orientations are roughly orthogonal with respect to the e_{hmax} orientations deduced from calcite *c*-axes (Fig. 5). However, these strain axis orientations cannot be coeval because *c*-axes (e_{hmax}) are related to the vein opening and twins (e_{hmin}) within a compressional regime. In this case, as the movement along the extensional basin bounding faults controlled the calcite micro-vein development and $e_{\mathrm{hmax}} - e_{\mathrm{hmin}}$ are orthogonal but not coeval, we propose that calcite twins were formed during the basin inversion along the same faults that produced the basin extension; furthermore, the slip vector on both extension and inversion processes must be very similar.

As is shown in Fig. 6, the NW–SE and E–W e_{hmin} orientations are found mainly close to the northern border of the basin and extend towards the basin interior only in the area where the basin thrusts over the Tertiary sediments (Figs. 2 and 6). In this area, e_{hmin} trends are also oriented perpendicular to the fold axes and cleavage traces identified by Casas-Saínz and Gil-Imaz (1998) and Gil-Imaz (1999). This parallelism suggests these structures are coeval and were developed during the basin inversion episode (Paleogene–Early Miocene; Casas-Saínz and Simón-Gómez, 1992). Calcite grains were undeformed since the Early Cretaceous and e-twins were most likely formed only close to the thrust ramp where the differential stresses were higher.

The N–S e_{hmin} trajectories (Fig. 6c) coincide in orientation with the shortening orientation deduced from fault analysis for the basin inversion episode (e.g. Casas-Saínz, 1990; Casas-Saínz and Simón-Gómez, 1992). This tectonic episode took place during the Oligocene–Middle Miocene interval (Casas-Saínz and Simón-Gómez, 1992). Thus, N–S

e_{hmin} trends are likely associated with the basin inversion during the Oligocene–Middle Miocene interval. The NW–SE e_{hmin} orientation strongly suggests other episodes of thrusting along NE–SW faults (Fig. 6d). Taking into account the shortening orientations deduced for the different tectonic episodes that took place in the Iberian Chain (Fig. 1c), the NW–SE e_{hmin} trajectories found here have the same orientation as that of the Middle–Late Miocene compression (Guadarrama compression), so this deformation is likely related to this tectonic episode, although the precise relationship is difficult to establish.

Thus, we can assume that the basin inversion took place in two episodes: (a) a first episode (Oligocene–Early Miocene) in which faults with a NW–SE orientation moved as thrusts (e.g. the northern border fault) and faults with a NE–SW trend probably had a wrench displacement (sinistral) (Fig. 7a and b); (b) a second episode (Guadarrama compression?) where the proposed fault displacement inverted, i.e. those NW–SE trending faults moved as wrench faults (dextral) and faults with a NE–SW orientation had a reverse slip (Fig. 7c). This episode probably took place in the Late Miocene, and taking into account the number of sites that show this deformation (Fig. 6c) and the foreland stratigraphic data (Casas-Saínz and Simón-Gómez, 1992), this episode has less importance than the former in the basin inversion history. The existence of strike-slip faults in both episodes could explain the principal strain orientations that suggest a wrench tectonic regime.

The E–W e_{hmin} orientations are found only in the inner part of the basin (Fig. 7b). As shown in Fig. 6b e_{hmin} orientations are also perpendicular to the fold axial planes and cleavage traces, suggesting that all these structures are coeval. The age of the tectonic event that generated all these structures is not clear. As was shown above, a deformational episode with a shortening direction oriented E–W has been inferred in other areas of the Iberian Chain (Castillian Branch and Altomira Range; e.g. Rodríguez-Pascua et al., 1994; Muñoz-Martín, 1997; González-Casado and García-Cuevas, 1999) during the Early–Middle Miocene (Fig. 1). Thus, the tectonic event that gave rise to this twinning could be related with this Early–Middle Miocene E–W tectonic episode.

Sites that show E–W shortening are superimposed in part over the chloritoid zone (Fig. 4). The metamorphism must predate the development of e-twins because temperatures during metamorphism (Casquet et al., 1992; Mata, 1997; Mantilla-Figueroa, 1999) are above type I e-twin temperature formation ($\leqslant$200 °C) and metamorphism took place before the Paleogene (radiometric ages yield values around 90 Ma; Golberg et al., 1988; Casquet et al., 1992; Mantilla-Figueroa, 1999).

5. Conclusions

Principal strain axis orientations calculated by means of calcite e-twin analysis and calcite *c*-axis orientations give a complete description of the different tectonic events recorded by micro-veins and their host rock. Spatial distribution of e-twins in the entire basin wedge show these microstructures to be developed only in the northern front, where the main thrust that controlled the basin inversion is located and where, probably, the maximum differential stress was reached.

As can be deduced from regional calcite *c*-axis orientations, during the Cameros basin extension period, two main dip-slip faults were active trending NW–SE and NE–SW rather than one NW–SE fault system as has been previously supposed (e.g. Casas-Saínz, 1990).

After calcite vein growth during Mesozoic extension, e-twins were formed during the Tertiary basin inversion episodes. The e_{hmin} orientations deduced here agree with the former tectonic inversion model proposed for this basin, i.e. a basin inversion related to a NW–SE south-west-dipping main thrust (Casas-Saínz, 1990) (northern Cameros thrust). At least one other thrusting episode where the former NW–SE faults move as dextral and thrusts faults have a NE–SW southeast-dipping orientation can be deduced from e-twins (Fig. 7). This second episode could have taken place during the Late Miocene (Guadarrama compression tectonic episode). The gentle folds and incipient cleavage located in the north part of this basin could be also related to the first tectonic episode described here. The perpendicularity between the micro-vein *c*-axis orientations and e_{hmin} trends suggests that the same faults controlled the basin extension and the two inversion episodes. Furthermore, the slip vectors during inversion and compression had the same orientation but, obviously, a different sense of movement.

The E–W e_{hmin} trends found in the central part of the studied area could be related to the Altomira tectonic episode, which suggests that this tectonic event would have a regional character and not a local one, as has been previously supposed (e.g. Muñoz-Martín et al., 1998).

The three e_{hmin} orientations deduced from e-twins coincide with the previously determined shortening directions of main tectonic episodes in the Iberian Chain, which show the utility of e-twin analysis for unravelling the complicated deformational and kinematic tectonic histories of the cover sequence.

Acknowledgements

The authors would like to thank A. Casas-Saínz, A. Gil-Imaz, C. Casquet and R. Mas for stimulating ideas and discussions about the Cameros basin geology. This paper is a part of the Ph.D. thesis of C. García-Cuevas and has been funded by the DGICYT projects number PB94-0242 and BTE2001-0998-C02-02. The manuscript was greatly improved by the review comments of Drs A. Meigs, R. Groshong and D. Fisher.

References

Alvaro, M., 1975. Estilolitos tectónicos y fases de plegamiento en el área de Sigüenza (borde del Sistema Central y de la Cordillera Ibérica). Estudios Geológicos 31, 241–247.

Alvaro, M., Capote, R., Vegas, R., 1979. Un modelo de evolución geotectónica para la Cadena Ibérica Oriental. Acta Geológica Hispánica 14, 172–177.

Arche, A., López-Gómez, J., 1996. Origin of the Permian–Triassic Iberian Basin, central-eastern Spain. Tectonophysics 226, 443–464.

Burkhard, M., 1993. Calcite twins, their geometry, appearance and significance as stress–strain markers and indicators of tectonic regime: a review. Journal Structural Geology 15, 351–368.

Calvo, J.P., Damms, R., Morales, J., López Martínez, N., Agustí, J., Anádon, P., Armenteros, I., Cabrera, L., Civis, J., Corrochano, A., Díaz Molina, M., Elizaga, E., Hoyos, M.M., Martínez, J., Moissenet, E., Muñoz, A., Pérez García, A., Pérez González, A., Portero, J.M., Robles, F., Santiesteban, C., Torres, T., Van der Meulen, A., Vera, J., Mein, P., 1993. Up-to-date Spanish continental Neogene synthesis and paleoclimatic interpretation. Revista de la Sociedad Geológica de España 6, 29–40.

Capote, R., 1983. La tectónica de la Cordillera Ibérica. In: Comba, J.A. (Ed.). Libro Jubilar J.M. Ríos. Instituto Geológico y Minero de España, Madrid, pp. 108–131.

Capote, R., Díaz, M., Gabaldón, V., Gómez, J.J., Sánchez de la Torre, L., Ruiz, P., Rossel, J., Sopeña, A., Yébenes, A., 1982. Evolución sedimentológica y tectónica del ciclo alpino en el tercio noroccidental de la Rama Castellana de la Cordillera Ibérica. Temas Geológicos Mineros 5, 1–290.

Casas-Saínz, A., 1990. El frente norte de las Sierras de Cameros. Estructuras cabalgantes y campo de esfuerzos. Ph.D. thesis, University of Zaragoza.

Casas-Saínz, A., Simón-Gómez, J.L., 1992. Stress field and thrust kinematics: a model for the tectonic inversion of the Cameros Massif (Spain). Journal of Structural Geology 14, 521–530.

Casas-Saínz, A., Gil-Imaz, A., 1998. Extensional subsidence, contractional folding and thrust inversion of the eastern Cameros basin, northern Spain. Geologische Rundschau 86, 802–818.

Casquet, C., Galindo, C., González-Casado, J.M., Alonso, A., Mas, J.R., Rodas, M., García, E., Barrenechea, J.F., 1992. El metamorfismo en la cuenca de Cameros. Geocronología e implicaciones tectónicas. Geogaceta 11, 22–25.

Craddock, J.P., van der Pluijm, B.A., 1988. Kinematic analysis of an en échelon–continuous vein complex. Journal of Structural Geology 10, 445–452.

Craddock, J.P., Nielson, K.J., Malone, D.H., 2000. Calcite twinning strain constraints on the emplacement rate and kinematic pattern of the upper plate of the Heart Mountain Detachment. Journal of Structural Geology 22, 983–991.

De Vicente, G., 1988. Análisis poblacional de fallas. El sector de enlace Sistema Central–Cordillera Ibérica. Ph.D. thesis, University Complutense of Madrid.

De Vicente, G., Calvo, J.P., Muñoz-Martín, A., 1996a. Neogene tectonosedimentary review of the Madrid Basin. In: Friend, P., Dabrio, C. (Eds.). Tertiary Basin of Spain. The Stratigraphic Record of Crustal Kinematics. Cambridge University Press, pp. 268–271.

De Vicente, G., Giner, J.L., Muñoz-Martín, A., González-Casado, J.M., Lindo, R., 1996b. Determination of present-day stress tensor and neotectonic interval in the Spanish Central System and Madrid Basin, central Spain. Tectonophysics 266, 405–424.

Evans, M.A., Dune, W.M., 1991. Strain factorization and partitioning in the North Mountain thrust sheet, central Appalachians, USA. Journal of Structural Geology 13, 21–35.

Evans, M.A., Groshong Jr, R.H., 1994. A computer program for the calcite strain-gauge technique. Journal of Structural Geology 16, 277–281.

Ferrill, D.A., 1991. Calcite twin width and intensities as metamorphic indicators in natural low-temperature deformation of limestone. Journal of Structural Geology 13, 667–675.

Ferrill, D.A., 1998. Critical re-evaluation of differential stress estimates from calcite twins in coarse-grained limestones. Tectonophysics 285, 77–86.

Ferrill, D.A., Groshong Jr, R.H., 1993a. Determination conditions in the northern Subalpine Chain, France, estimated from deformations modes in coarse-grained limestones. Journal of Structural Geology 15, 995–1006.

Ferrill, D.A., Groshong Jr, R.H., 1993b. Kinematic model for the curvature of the northern Subalpine Chain, France. Journal of Structural Geology 15, 523–541.

García-Cuevas, C., 2000. Análisis de la deformación en la Cordillera Ibérica a partir del estudio del maclado de la calcita. Ph.D. thesis. University Complutense of Madrid.

Gil-Imaz, A., 1999. La estructura de la Sierra de Cameros: deformación dúctil y su significado a escala cortical. Ph.D. thesis. Universidad of Zaragoza.

Golberg, J.M., Guiraud, M., Maluski, H., Séguret, M., 1988. Caractères pétrologuiques et âge du métamorphisme en contexte distensif du bassin sur décrochement de Soria (Crétacé Inferieur, Nord Espagne). Comtes Rendus de l'Academie des Sciences Paris 307, 521–527.

González-Casado, J.M., García-Cuevas, C., 1999. Calcite twins from micro-veins as indicators of deformation history. Journal of Structural Geology 21, 875–889.

González-Casado, J.M., Caballero, J.M., Casquet, C., Galindo, C., Tornos, F., 1996. Palaeostress and geotectonic interpretation of the Alpine Cycle onset in the Sierra del Gudarrama (eastern Iberian Central System), based on evidence from episyenites. Tectonophysics 262, 213–229.

Groshong Jr, R.H., 1972. Strain calculated from twinning in calcite. Geological Society of America Bulletin 83, 2025–2048.

Groshong Jr, R.H., 1974. Experimental test of the least-squares strain gauge calculation using twinned calcite. Geological Society of America Bulletin 85, 1855–1864.

Groshong Jr, R.H., 1975. Strain, fractures and pressure solution in natural single-layer folds. Geological Society of America Bulletin 86, 1363–1376.

Groshong Jr, R.H., Pfiffner, O.A., Pringle, L.R., 1984. Strain partitioning in the Helvetic thrust belt of eastern Switzerland from the leading edge to the internal zone. Journal of Structural Geology 6, 19–32.

Guimerà, J., Alvaro, M., 1990. Structure et évolution de la compression alpine dans la Chaîne Ibérique et la Chaîne Cotière Catalane (Espagne). Bulletin de la Société Geologique de France 8, 339–348.

Guimerà, J., Alonso, A., Mas, J.R., 1995. Inversion of an extensional–ramp basin by a newly formed thrust: the Cameros basin (N. Spain). In: Buchanan, J.G., Buchanan, P.G. (Eds.), Basin Inversion. Geological Society Special Publication 88, pp. 433–453.

Guiraud, M., Séguret, M., 1985. Releasing solitary overstep model for the Late Jurassic–Early Cretaceous (Wealden) Soria strike-slip basin (North Spain). In: Biddle, K.T., Christie-Blick N. (Eds.), Strike-slip Deformation, Basin Formation and Sedimentation. Special Publication Society of Economic Paleontologists and Mineralogists 37, pp. 159–175.

Harris, J.H., van der Pluijm, B.A., 1998. Relative timing of calcite twinning strain and fold–thrust belt development; Hudson Valley fold–thrust belt, New York, USA. Journal of Structural Geology 20, 21–23.

Hindle, D.A., 1997. Quantify stresses and strains from the Jura Arc, and their usefulness in choosing and deformation model for the region. Ph.D. thesis. University of Neuchatel.

Kilsdonk, B., Wiltschko, D.V., 1988. Deformation mechanisms in the southeastern ramp region of the Pine Mountain block, Tennessee. Geological Society of America Bulletin 100, 653–664.

Laurent, Ph., Bernard, Ph., Vasseur, G., Etchecopar, A., 1981. Stress tensor determination from the study of e-twins in calcite: a linear programming method. Tectonophysics 78, 651–660.

Laurent, Ph., Tourneret, C., Laborde, O., 1990. Determining deviatoric

stress tensors from calcite twins: applications to monophased synthetic and natural polycrystals. Tectonics 9, 379–389.

Lee, J.C., Angelier, J., 1994. Paleostress trajectory maps based on the results of local determinations: the "Lissage" program. Computers and Geosciences 20, 161–191.

Mantilla-Figueroa, L.C., 1999. El metamorfismo hidrotermal de la Sierra de Cameros (La Rioja–España): petrología, geoquímica, geocronología y contexto estructural de los procesos de interación fluido-roca. Ph.D. thesis. University Complutense of Madrid.

Marqués, L., Maestro, A., Gil, A., Casas, A.M., 1996. Aportaciones del análisis microestructural a la evolución tectónica del extremo oriental de la Cuenca de Cameros. Geogaceta 20 (4), 767–769.

Mas, R., Alonso, A., Guimerà, J., 1993. Evolución tectonosedimentaria de una cuenca extensional intraplaca: la cuenca finijurásica-eocretácica de Los Cameros (La Rioja–Soria). Revista de la Sociedad Geológica de España 6, 129–144.

Mata, M.P., 1997. Caracterización y evolución mineralógica de la cuenca mesozoica de Cameros (Soria–La Rioja). Ph.D. thesis. University of Zaragoza.

Miegebielle, V., Hervouet, Y., Xavier, J.P., 1993. Analyse structurale de la partie méridionale du bassin de Soria (Espagne). Bulletin des Centres de Recherches Exploration–Production Elf–Aquitaine 17, 19–37.

Mosar, J., 1989. Deformation interne dans les Préalpes Médianes (Suisse). Eclogae Geologicae Helvetiae 82, 765–794.

Muñoz-Martín, A., 1997. Evolución geodinámica del borde oriental de la Cuenca del Tajo desde el Oligoceno hasta la actualidad. Ph.D. thesis. University Complutense of Madrid.

Muñoz-Martín, A., Cloetingh, S., De Vicente, G., Andeweg, B., 1998. Finite-element modelling of Tertiary paleostress fields in the eastern part of the Tajo Basin (central Spain). Tectonophysics 300, 47–62.

Nemcok, M., Kovác, D., Lisle, R.J., 1999. A stress inversion procedure for polyphase calcite twin and faults/slip data sets. Journal of Structural Geology 21, 597–611.

Pfiffner, O.A., Burkhard, M., 1987. Determination of paleostress axes orientations from fault, twin and earthquake data. Annales Tectonicae 1, 48–57.

Platt, N.H., 1990. Basin evolution and fault reactivation in the western Cameros basin, Northern Spain. Journal of the Geological Society London 147, 165–175.

Rodríguez-Pascua, M.A., De Vicente, G., González-Casado, J.M., 1994. Cinemática y dinámica de las deformaciones de la zona del Alto Tajo (Guadalajara). Cuadernos do Laboratorio Xeologico de Laxe 19, 163–174.

Salas, R., Casas, A., 1993. Mesozoic extensional tectonics, stratigraphy and crustal evolution during the Alpine cycle of the eastern Iberian Chain. Tectonophysics 228, 33–55.

Simón-Gómez, J.L., 1986. Analysis of a gradual change in stress regime (example from the eastern Iberian Chain, Spain). Tectonophysics 124, 37–53.

Spang, J.H., 1972. Numerical method for dynamic analysis of calcite twin lamellae. Geological Society of America Bulletin 83, 467–472.

Spang, J.H., Groshong Jr, R.H., 1981. Deformation mechanisms and strain history of a minor fold from the Appalachian Valley and Ridge province. Tectonophysics 72, 323–342.

Teufel, L.W., 1980. Strain analysis of experimentally superposed deformation using calcite twin lamellae. Tectonophysics 65, 291–309.

Tischer, G., 1966. Über die Wealden–Ablagerung and ide Tektonik der östlichen de los Cameros in den nordwestlichen Iberischen Ketten (Spanien). Geologisches Jahrbuch Biehefte 44, 123–164.

Turner, F.J., 1953. Nature and dynamic interpretation of deformation lamellae in calcite of three marbles. American Journal of Science 251, 276–298.

Viallard, P., 1983. Le décollement de couverture dans la Chaîne Ibérique méridionale (Espagne): effet de raccourcissements differentiels entre substratum et couverture. Bulletin de Société Géologique de la France 7, 379–387.

Vilas, L., Alonso, A., Arias, C., García, A., Mas, J.R., Rincón, R., Meléndez, N., 1983. The Cretaceous of the South-western Iberian Ranges (Spain). Zittelania 10, 245–254.

Weiss, L.E., 1954. A study of tectonic style: structural investigation of a marble quartzite complex in southern California. University of California Publications in Geological Science 30, 1–102.

Wiltschko, D.V., Medwedeff, D.A., Millson, H.E., 1985. Distribution and mechanisms of strain within rocks on the northwest ramp of Pine Mountain block, southern Appalachian foreland: a field test of theory. Geological Society of America Bulletin 96, 426–435.